Current Research in Insect Science 5 (2024) 100082

Contents lists available at ScienceDirect

Current Research in Insect Science

journal homepage: www.elsevier.com/locate/cris

Arthropod repellent interactions with olfactory receptors and ionotropic receptors analyzed by molecular modeling

Robert Renthal

Department of Neuroscience, Developmental and Regenerative Biology, University of Texas at San Antonio, San Antonio, TX, United States

ARTICLE INFO

Keywords:
Olfactory receptors
Gustatory receptors
Ionotropic receptors
Molecular modeling
Ligand docking

ABSTRACT

The main insect chemoreceptors are olfactory receptors (ORs), gustatory receptors (GRs) and ionotropic receptors (IRs). The odorant binding sites of many insect ORs appear to be occluded and inaccessible from the surface of the receptor protein, based on the three-dimensional structure of OR5 from the jumping bristletail *Machilis hrabei* (*Mhra*OR5) and a survey of a sample of vinegar fly (*Drosophila melanogaster*) OR structures obtained from artificial intellegence (A.I.) modeling. Molecular dynamics simulations revealed that the occluded site can become accessible through tunnels that transiently open and close. The present study extends this analysis to examine seventeen ORs and one GR docking with ligands that have known valence: nine that signal attraction and nine that signal aversion. All but one of the receptors displayed occluded ligand binding sites analogous to *Mhra*OR5, and docking software predicted the known attractant and repellent ligands will bind to the occluded sites. Docking of the repellent DEET was examined, and more than half of the OR ligand sites were predicted to bind DEET, including receptors that signal aversion as well as those that signal attraction. However, DEET may not actually have access to all the attractant binding sites. The larger size and lower flexibility of repellent molecules may restrict their passage through the tunnel bottlenecks, which could act as filters to select access to the ligand binding sites. In contrast to ORs and GRs, the IR ligand binding site is in an extracellular domain known to undergo a large conformational change from an open to a closed state. A.I. models of two *D. melanogaster* IRs of known valence and two blacklegged tick (*Ixodes scapularis*) IRs having unknown ligands were computationally tested for attractant and repellent binding. The ligand-binding sites in the closed state appear inaccessible to the protein surface, so attractants and repellents must bind initially at an accessible site in the open state before triggering the conformational change. In some IRs, repellent binding sites were identified at exterior sites adjacent to the ligand-binding site. These may be allosteric sites that, when occupied by repellents, can stabilize the open state of an attractant IR, or stabilize the closed state of an IR in the absence of its activating ligand. The model of *D. melanogaster* IR64a suggests a possible molecular mechanism for the activation of this IR by H^+. The amino acids involved in this proposed mechanism are conserved in IR64a from several Dipteran pest species and disease vectors, potentially offering a route to discovery of new repellents that act via the allosteric site.

1. Introduction

Arthropod repellents act through chemosensory pathways (Renthal, 2021). Action potentials in chemosensory neurons are triggered by chemosensory receptors interacting with chemicals captured from the environment. DEET has been demonstrated to cause action potentials in chemosensory neurons of insect antennae, palps and labellae (Lee et al., 2010; Syed et al., 2011; Guo et al., 2020) (although there is also evidence for DEET suppression of the volatility of odorants (Afify et al., 2019)). Three main types of arthropod chemosensory receptors have been identified: olfactory receptors (ORs), gustatory receptors (GRs) and ionotropic receptors (IRs). ORs are unique heteromeric ligand-gated ion channels that are found in insect antennae and palps (Su et al., 2009). GRs are homomeric ligand-gated ion channels related to ORs, found in insects mostly on labellae and tarsi and also found in a wide variety of invertebrates (Robertson, 2015). IRs resemble ionotropic glutamate receptors, and they are found in the antenna, labella, pharynx and tarsi of insects and in the fore tarsi of acari (Rytz et al., 2013; Lei et al., 2019). The understanding of these chemoreceptors at the molecular level could provide new information for design of improved attractants and

E-mail address: robert.renthal@utsa.edu.

https://doi.org/10.1016/j.cris.2024.100082
Received 23 December 2023; Received in revised form 29 April 2024; Accepted 1 May 2024
Available online 3 May 2024

repellents, perhaps narrowing the repellency to targeted pest species.

Currently, there are two cryo-EM structures for insect ORs (Butterwick et al., 2018; Del Marmol et al., 2021), one of which provides insight into the molecular interaction between the receptor protein and the channel-gating ligand. The structure of an odorant bound to OR5 of the jumping bristletail *Machilis hrabei* (Del Marmol et al., 2021) holds important clues about the ligand-binding and gating mechanisms. The ion channel is open in the ligand-bound structure, suggesting that *Mhrara*OR5 does not, by itself, undergo rapid desensitization after ligand binding, unlike ion channels such as the nicotinic acetylcholine receptor (Yakel, 2010). A notable feature of the *Mhra*OR5 ligand binding site is that it is completely occluded, having no access to the protein surface. Using molecular dynamics simulation, we recently identified tunnels, leading from the *Mhra*OR5 ligand binding site to the protein surface, that open and close on a nanosecond time scale (Renthal and Chen, 2022). These results suggest possible routes for the ligand into or out of its binding site via the lipid bilayer or the extracellular protein surface. Alternatively, there may be another conformation of *Mhra*OR5, not yet observed, in which the ion channel is closed and the ligand-binding site is open. Assuming that the tunnels are the path into and out from the ligand binding site, we asked whether this is a general property of ORs, or particular to *Mhra*OR5. We examined 21 AlphaFold structures of vinegar fly (*Drosophila melanogaster*) ORs that have known ligands. In 20 structures, the ligand binding sites predicted by AutoDock software were analogous to the ligand binding site detected in *Mhra*OR5, and in 19 there was evidence for tunnels similar to those we found in *Mhra*OR5 (Renthal and Chen, 2022). In several cases we were surprised that AutoDock predicted binding of DEET to the same OR binding pocket as ligands known to elicit attraction behavior. This seemed to be consistent with predictions that repellents act as "confusants", activating and inhibiting a pattern of receptors that cannot be interpreted by the insect brain (DeGennaro, 2015). Considering the large amount of behavioral and physiological data on *D. melanogaster* attractants and repellents, it seems worthwhile to extend this analysis to a sample of ORs for which attractant or repellent behavioral responses have been determined.

Compared to insect ORs, far less structural information is available for arthropod IRs: no molecular structures are yet known. Nevertheless, the similarities of IRs to ionotropic glutamate receptors (GluRs) provides some possibilities for analysis of ligand interactions with IRs. The ligand-binding domains (LBDs) of the ionotropic GluR2 receptor, when heterologously expressed independent of the ion channel and other domains, were found to retain nearly the same ligand-binding activity as intact receptors (Kuusinen et al., 1995). The LBDs are shaped like clam shells, and they have two different conformations: open, in the absence of ligand, and closed, in the presence of ligand (Armstrong and Gouaux, 2000). Many crystal structures of GluR LBDs and LBD homologs have been determined from a variety of organisms, ranging from humans to bacteria, and all have highly similar three-dimensional folds, despite the low levels of amino acid sequence identity.

In this report, I have used artificial intelligence (A.I.)-based protein structure modeling and computed ligand docking to extended our previous analysis of *D. melanogaster* ORs to 17 ORs and 1 GR that have known valence. Also, I have used similar methods to examine structural models of *D. melanogaster* and *Ixodes scapularis* (blacklegged tick) IRs. The results provide new insights into the molecular mechanisms of repellency mediated by ORs, GRs and IRs.

2. Methods

Seventeen ORs and one GR from *D. melanogaster* were selected for analysis based on documented behavioral responses (Weiss et al., 2011; Thoma et al., 2014; Joseph and Carlson, 2015; Badel et al., 2016; Brown et al., 2017; Mohamed et al., 2019), and ligands were selected from the strongest known responses in the OR or GR tuning profiles (Munch and Galizia, 2016). Not all of the ORs analyzed here are narrowly tuned, so the valence attributed to some of the odors may be combinatorial. AlphaFold2 (AF) models (Jumper et al., 2021) of the receptors (Table S1, Supplementary Material 1) were downloaded from Uniprot (https://www.uniprot.org/) and processed to AutoDock pdbqt format using AutoDock Tools (version 1.5.7, https://ccsb.scripps.edu/mgltools/) (Morris et al., 2009). AF models of *D. melanogaster* IRs and *I. scapularis* IRs (Table S1, Supplementary Material 1, and Supplementary Material 2) were obtained from Uniprot or generated on local servers, and the same sequences were submitted to Robetta (https://robetta.bakerlab.org/) to obtain RoseTTAFold (RF) models (Baek et al., 2021). Model quality was assessed using QMEANDisCo (Studer et al., 2020). The average QMEANDisCo values for the models were typically 0.55 - 0.60, compared to 0.8 for crystal structures. The apparent lower quality of the A.I. models is largely due to disordered loops that are included in the computed models but are mostly absent from crystal structures. The conformational states of the models' ligand-binding domains (LBDs) were assessed using the center-of-mass coordinates ξ_1 and ξ_2 described for the rat ionotropic glutamate receptor GluR2 (Lau and Roux, 2007). The amino acids in a particular IR which correspond to the conformational-state sensitive positions of GluR2 that comprise ξ_1 and ξ_2 were identified by superimposing the rat GluR2 LBD crystal structures of the open and closed conformations (Protein Data Bank IDs 1fto and 1ftj, respectively), using PyMOL software (Schrodinger, New York, NY). Center-of-mass calculations of the atomic coordinates of these amino acids were carried out using the "measure inertia" command in the Tk Console of VMD software (Humphrey et al., 1996). The sequence positions, the ξ_1 and ξ_2 coordinates, and the open/closed distance measurements are given in Supplementary Material 3, and the distances are summarized in Table S2, Supplementary Material 1. The Tk Console commands and output are given in Supplementary Material 4.

For molecular docking analysis, models were converted from pdb to AutoDock pdbqt format using AutoDock Tools. This conversion can also be done using Open Babel software (https://sourceforge.net/projects/openbabel/). Ligand structures were obtained from PubChem (https://pubchem.ncbi.nlm.nih.gov/), converted from sdf to pdb format with PyMOL, and then processed to AutoDock pdbqt format with AutoDockTools. Ligand docking to each model was calculated using AutoDock Vina (version 1_1_2_mac (Trott and Olson, 2010)). Calculations typically used a grid box of about 40 Å centered on the transmembrane region (ORs and GRs) or the LBD (IRs), and the exhaustiveness parameter was set to 32. The results in Tables 1 and 3 list the highest probability AutoDock docking sites. The AutoDock Vina command lines, showing the parameters used, along with the output giving the atomic coordinates of the docked ligand, are provided in Supplementary Material 4. The ligand dimensions in Table 2 were measured with ImageJ (Schneider et al., 2012) using images of CPK representations from Jmol (https://jmol.sourceforge.net/) that contained bond length calibration marks. The OR and GR docking sites predicted by AutoDock were superimposed on a surface representation of the protein structures, using PyMOL, to examine the shapes of the binding pockets and their connecting tunnels. A representative example is shown in Fig. 1.

3. Results

3.1. Drosophila OR/GR receptors

Eighteen receptors were selected, 17 ORs and 1 GR, of which 9 are known to stimulate attraction and 9 are known to stimulate aversion (Table 1). For each receptor, the ligand with the strongest known electrophysiological response (Munch and Galizia, 2016) was selected for molecular docking analysis. In 17 of 18 receptors, the highest probability binding site found by AutoDock was analogous to the location of the ligand-binding site identified in the cryo-EM structure of *Mhra*OR5. The predicted site that was not analogous to *Mhra*OR5 was located on

Table 1
AutoDock Analysis of Ligand Binding to AlphaFold2 Models of *D. melanogaster* OR/ GR Receptors.

OR	Ligand	Attr./ Repel[a]	Ligand site[b]	DEET site[c]	Ligand affinity[d]	DEET affinity[d]
7a	E2-hexenal	R	I	O	−4.4	−6.3
9a	3-hydroxy-2-butanone	A	I	I	−4.2	−7.6
10a	methyl salicylate	R	I	I	−6.8	−7.1
33c	cyclohexanone	R	O	O	−4.6	−6.0
35a	1-octanol	R	I	O	−4.3	−5.6
42a	ethylbutyrate	A	I	I	−4.8	−6.4
42b	3-hexanone	A	I	O	−4.4	−5.2
46a	4-methyl phenol	R	I	I	−5.9	−6.6
49b	2-methyl phenol	R	I	I	−5.5	−6.2
56a	geosmin	R	I	O	−6.8	−6.5
59b	ethyl acetate	A	I	I	−3.6	−6.7
67c	ethyl lactate	A	I	S	−5.2	−6.2
71a	ethylguaiacol	A	I	I	−6.4	−6.9
85d	isopentyl acetate	A	I	O	−5.5	−6.3
85e	fenchone	R	I	I	−5.8	−6.9
92a	butanedione	A	I	O	−4.2	−5.8
98a	ethyl benzoate	A	I	I	−6.3	−7.1
GR						
66a	caffeine	R	I	I	−6.1	−6.3

Notes: a) A, attractant; R, repellent. b) I, ligand predicted to bind to interior site analogous to eugenol site in *Mhra*OR5; O, ligand predicted to bind to a site other than the *Mhra*OR5-like interior site. c) I, DEET predicted to bind to interior site analogous to eugenol site in *Mhra*OR5; O, DEET predicted to bind to a site other than the *Mhra*OR5-like interior site; S, DEET predicted to bind to interior site between the ligand site and the extracellular protein surface. d) predicted free energy change of ligand binding, Kcal/mol.

the OR surface that contacts the hydrocarbon chains of the lipid bilayer. AutoDock was also used to predict the highest probability DEET binding sites. In all but one case, AutoDock predicted that DEET binds to the OR or GR with a higher affinity than the natural ligand (Table 1). AutoDock predicted that DEET binding overlaps with the natural ligand binding site in nine ORs and one GR, but in eight ORs the DEET binding site was predicted to be different from the natural ligand site (Table 1 and Fig. 2). Of the non-overlapping sites, four were in ORs that stimulated aversion and four that stimulated attraction. Of the ten sites that overlap with DEET binding, five sites were in aversive and five in attractive receptors.

Predicted binding of DEET to receptors known to stimulate attraction would seem to confirm the concept of DEET as a "confusant" (Pellegrino et al., 2011; DeGennaro, 2015). However, only one of the five attractant ORs that AutoDock predicts to bind DEET, *Dmel*OR42a, has been shown experimentally to respond to DEET (Syed et al., 2011), and one, *Dmel*OR59b, has been shown not to respond to DEET (Pellegrino et al., 2011). To understand this perhaps puzzling data, it is important to consider that AutoDock predicts whether a molecule fits into a surface or occluded binding pocket of a protein, but it does not evaluate whether a particular site is actually accessible. Our recent finding of transiently opening tunnels in *Mhra*OR5 that connect the protein surface to the occluded ligand-binding site (Renthal and Chen, 2022) might help explain, in part, why repellents don't necessarily activate attraction by binding to receptors for attractants. It is possible that tunnels could act as filters to exclude binding of some ligands. In other words, although the repellent DEET can be modeled to bind to the same ligand site as some attractants, DEET may be physically restricted from diffusing from the protein surface to the interior binding site. Filters based on electrostatic interactions are known in ion channels (Doyle et al., 1998), but the ligands being considered here are all non-ionic and relatively non-polar. Two other molecular properties that could be involved in filtering are shape and flexibility. In our molecular dynamics simulations of *Mhra*OR5 we observed that the tunnels to the ligand-binding site were blocked by transiently opening bottlenecks that acted like gates (Renthal and Chen, 2022). Therefore, the minimum cross-sectional areas of the ligands might be a selection property for a filter, like the mesh size in a sieve. The minimum height and width was measured for each of the ligands of ORs 9a, 42a, 59b, 71a and 98a (Table 2). In addition, because the tunnels observed in *Mhra*OR5 had turns, it is possible that molecular flexibility would be a necessary property for diffusion through the tunnel. As a proxy for flexibility, the percentage of rotatable C—C, C—O and C—N bonds (excluding methyls, carbonyls and alcohols) was determined (Table 2). These results were compared with the ligands of the four ORs (*Dmel*10a, *Dmel*46a, *Dmel*49b, *Dmel*85e) and one GR (*Dmel*66a) for which DEET was predicted to bind to the same interior site as the repellent ligands (Table 2). Qualitatively, it is apparent that DEET and the naturally repellent ligands are larger and less flexible than the attractant ligands. This can be seen graphically in the 3D plot in Fig. 3, where the attractants and repellents cluster in non-overlapping regions of size-flexibility space. These results support the idea that in many cases DEET may be excluded from attractant ORs but it could bind more generally to aversive ORs and GRs.

Some of the predicted interior ligand binding sites are completely occluded, and others are connected to the exterior surface and/or the lateral surface by a variety of narrow tunnels or shafts. A few of the connections end in pockets on the exterior surface. The exterior pockets point to the possibility of additional ligand binding sites. For example, AutoDock modeling shows that the interior ligand site of *Dmel*OR59b can accommodate two molecules of ethyl acetate, both with the same affinity, and more ethyl acetate is modeled to bind to two exterior surface pockets above the interior ligand binding site (Fig. 1B). These

Table 2
Molecular properties of attractants and repellents.

		Height[a]	Thickness[a]	Rotatable[b]	Total bonds[b]	Fraction rotatable
Receptor	Attractant					
*Dmel*OR9a	3-hydroxy-2-butanone	0.574	0.559	1	1	1.0
*Dmel*OR42a	ethyl butyrate	0.598	0.420	4	4	1.0
*Dmel*OR59b	ethyl acetate	0.554	0.397	2	2	1.0
*Dmel*OR71a	ethylguaiacol	0.791	0.388	2	8	0.3
*Dmel*OR98a	ethyl benzoate	0.678	0.419	3	9	0.3
Receptor	Repellent					
*Dmel*OR10a	methyl salicylate	0.789	0.663	2	8	0.3
*Dmel*OR46a	4-methyl phenol	0.650	0.361	0	6	0.0
*Dmel*OR49b	2-methyl phenol	0.698	0.381	0	6	0.0
*Dmel*OR85e	fenchone	0.674	0.727	0	8	0.0
*Dmel*GR66a	caffeine	0.868	0.402	0	10	0.0
	DEET	0.857	0.603	4	10	0.4

Footnotes: a) nm; b) C—C, C—O and C—N, excluding methyls, carbonyls and alcohols.

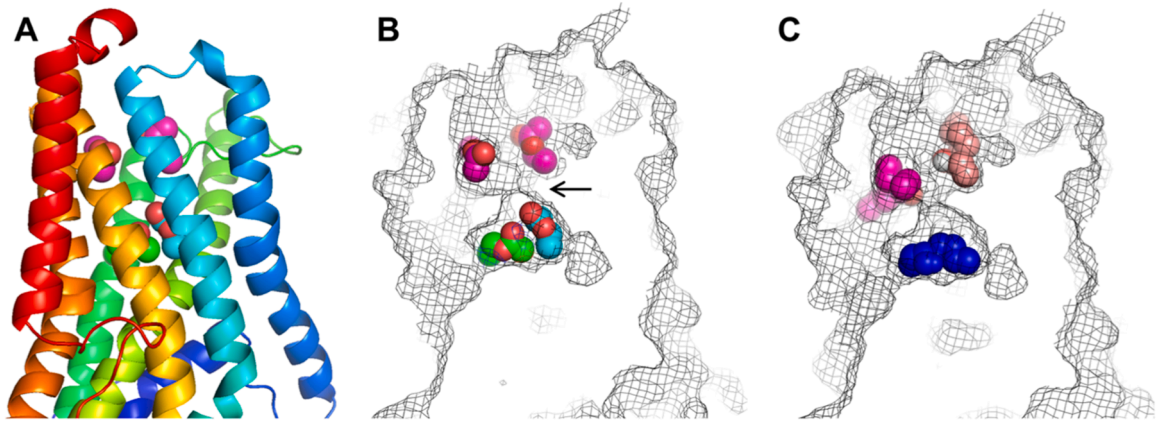

Fig. 1. Modeled ligand-binding sites in OR59b. Model is AF-Q9W1P8-F1-model_v4. A) Helix cartoon showing the view in panels B and C. Helices are in rainbow colors from N-terminus (blue) to C-terminus (red). Helix orientation is roughly perpendicular to plane of olfactory receptor neuron membrane. Top of structure is extracellular surface; bottom is truncated just below the inner surface of the lipid bilayer. Four bound ethyl acetate molecules, in sites identified by AutoDock, are depicted by their atomic surface. B) Cut-away view, in the same orientation as panel A. Two ethyl acetate molecules in the interior binding site are colored with red oxygens and green or cyan carbons. Two ethyl acetate molecules in the exterior surface binding site are colored with red oxygens and magenta carbons. Arrow identifies bottleneck between exterior site and interior site. Molecular surface of OR59b shown in mesh representation. C) Same view as panels A and B, except ligand sites show the positions of two molecules of 1-octen-3-ol (blue and tan) and one molecule of DEET (magenta), predicted by AutoDock.

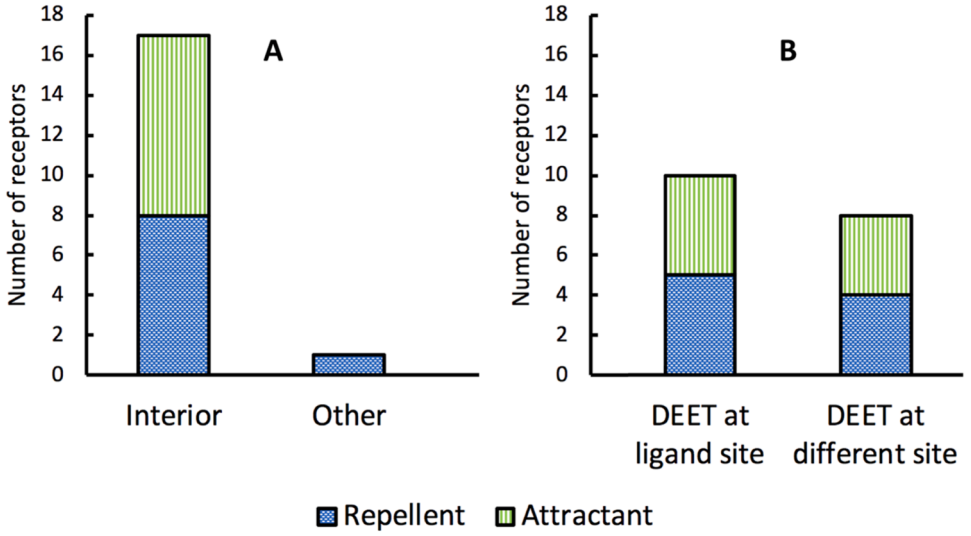

Fig. 2. Analysis of ligand binding sites of 17 ORs and 1 GR from *D. melanogaster*. Graph bars are separated into segments based on numbers of sites on receptors known to be stimulated by attractants or repellents. A) Ligand binding sites predicted by AutoDock are classified as interior if they are analogous to the known ligand binding site in *Mhra*OR5. B) DEET binding sites predicted by AutoDock to be either at the same site as the ligand or at a different site.

multiple binding sites may indicate the occurrence of cooperative ligand binding. Although DEET fits into the interior binding site, the bottleneck between the surface and interior sites (Fig. 1B) appears to be too narrow for DEET to enter the interior. Thus, by itself, DEET does not activate the *Dmel*OR59b ion channel (Pellegrino et al., 2011). The weak ligand, 1-octen-3-ol, is modeled by AutoDock to fill the entire interior site and also bind in the exterior surface sites (Fig. 1C). AutoDock predicts that DEET also can bind in the surface sites. The function of the surface sites may be inferred from the report that DEET enhances 1-octen-3-ol activation of *Dmel*OR59b, (Pellegrino et al., 2011), suggesting that the exterior sites may be involved in modulating the frequency of channel-opening.

3.2. *Drosophila* IRs

Unlike the ORs, which appear to undergo only small conformational changes after ligand binding (Del Marmol et al., 2021), the ionotropic glutamate receptor LBD shows 0.4 nm closure in the vicinity of the ligand binding site when glutamate binds (Lau and Roux, 2007). Therefore, the size of the LBD clam shell opening was used to assess the conformational state of the LBD in the models, as shown in Supplementary Table S2. For unknown reasons, most AlphaFold (AF) LBD models are in the open conformation, and many RosettaFold (RF) models of the same sequence are in the closed conformation. I selected two *D. melanogaster* IRs that have open AF models and closed RF models, in order to compare ligand binding to an IR that transduces aversion (*Dmel*IR64a) and IR that transduces attraction (*Dmel*IR20a).

*Dmel*IR64a is expressed in the sacculus of the antenna along with its coreceptor *Dmel*IR8a (Ai et al., 2013). *Dmel*IR64a is activated by acidity to produce an aversive response (Ai et al., 2010). The molecular basis of this response to acidity is unknown, but it appears to be initiated by H^+, since the neuron containing IR64a responds to HCl (Ai et al., 2010). Inspection of the model for the closed conformation reveals that the site analogous to the glutamate-binding site of iGluR2 is occupied by the side chain of Tyr 134 (LBD sequence; residue 627 in the full sequence, NP_647,962.1, numbered assuming cleavage of a 15 amino acid signal

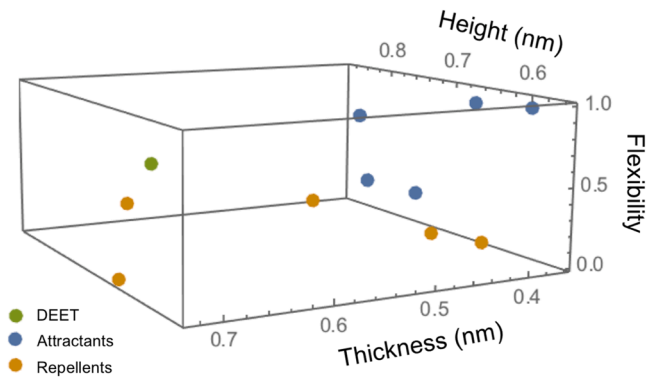

Fig. 3. Three dimensional graph of molecular properties of receptor ligands. Attractants (blue circles) are clustered in a region of higher flexibility and smaller size than repellents (tan circles and DEET, green circle). Height and thickness axes are in units of nanometers, and flexibility is in units of fraction of rotatable bonds.

sequence) (Fig. 4B). The side chain of the conserved LBD Arg 89 (387 in the full sequence) is oriented away from interaction with this site, in contrast to its normal interaction with the bound ligand. Tyr 134 (627) is arranged differently in the open conformation, where it is rotated 120° away from the ligand site and its OH group comes within H-bonding distance of the Asn 135 (628) side chain amide carbonyl (3.2 Å) (Fig. 4A). The rotated position of Tyr 134 also appears to be stabilized by a H-bond between the Asn 135 amide and His 222 (715) (3.4 Å). However, in the closed conformation, the Asn-His H-bond is broken (4.8 Å). These differences suggest a possible molecular mechanism for the detection of H^+ by *Dm*IR64a. When protonated at low pH, His 222 would no longer be a H-bond acceptor for Asn 135, thus weakening the interaction between Asn 135 and Tyr 134, releasing the Tyr-phenolic side chain and allowing it to move into the ligand-binding site as a sort of internal ligand. It is possible that repellents could be found that would drive this activation process, thereby mimicking H^+ and stimulating an aversive behavioral response. AutoDock predicts a binding site for several different repellents in a cavity located above and to the right of the cleft separating the two clam shell domains (view facing the cleft with the transmembrane domains downwards) (Supplementary Table S2), in the closed conformation.

*Dmel*IR20a is expressed in the pharynx (Sánchez-Alcañiz et al., 2018; Koh et al., 2014; Chen and Dahanukar, 2017; Joseph et al., 2017), abdomen (Koh et al., 2014;), and tarsal sensilla (Ganguly et al., 2017; Sánchez-Alcañiz et al., 2018; Koh et al., 2014). Ion channels composed of *Dmel*IR20a and *Dmel*IR76b are activated by amino acids: primarily serine, phenylalanine and threonine (Ganguly et al., 2017). These amino acids trigger an attraction behavioral response mediated by the *Dmel*IR20a tuning receptor. Autodock modeling shows Ser, Phe-and Thr-bind to a pocket in the closed state that is analogous to the Glu-binding site in the GluR2 LBD (Table 3). The ligand binding site has small openings to the protein surface at the right and left sides of the ligand-binding pocket, a feature not observed in other closed state models examined in this study. Ser, Thr-and Phe-also bind to sites in the open LBD conformation that are near the region that forms the binding pocket in the closed conformation, suggesting a possible pathway for ligand binding. Autodock predicts that many repellents bind to the same region of the open LBD conformation, but only DEET and IR3535 bind in the pocket of the closed LBD (Table 3). This suggests a mechanism whereby some repellents could be rejected by receptors that trigger attraction. However, in the case of *Dmel*IR20a, the possibility of DEET and IR3535 activation of attraction responses is consistent with the "confusant" model for repellency (Pellegrino et al., 2011; DeGennaro, 2015).

3.3. Tick IRs

Tick chemosensory reception occurs primarily in the Haller's organ of the fore tarsus and the palps of the capitulum. A transcriptomics analysis of the blacklegged tick, *I. scapularis*, found 99 IRs that were expressed at various levels in the fore tarsus (Josek et al., 2018). Of these, 22 have expression levels greater than 3 counts per kilobase. LBDs of *Isca*IR119 and *Isca*IR141 were modeled by AlphaFold and found to be in the open state, and the corresponding RoseTTAFold models were found to be in the closed state (Table S2). The LBD models were computationally tested for binding to picaridin, IR3535, and p-menthane-3,8- diol, which have been shown to have repellent activity against *Ixodes* ticks (Dautel et al., 2013), and p-cresol, which may be an attractant at low amounts and a repellent at higher amounts (Wood et al., 1975; Josek et al., 2021). Binding was also modelled for butyrate and γ-valerolactone, which have been shown to be attractants for *Ixodes* ticks (Leonovich, 2004; Faraone et al., 2020), and guanine, which has been found to be attractive to many tick species, including *I. scapularis* (Sonenshine et al., 2003). Menthanediol, p-cresol, valerolactone, butyrate, and guanine were predicted to bind to the open state of *Isca*IR119. However, only butyrate, valerolactone, and p-cresol were predicted to

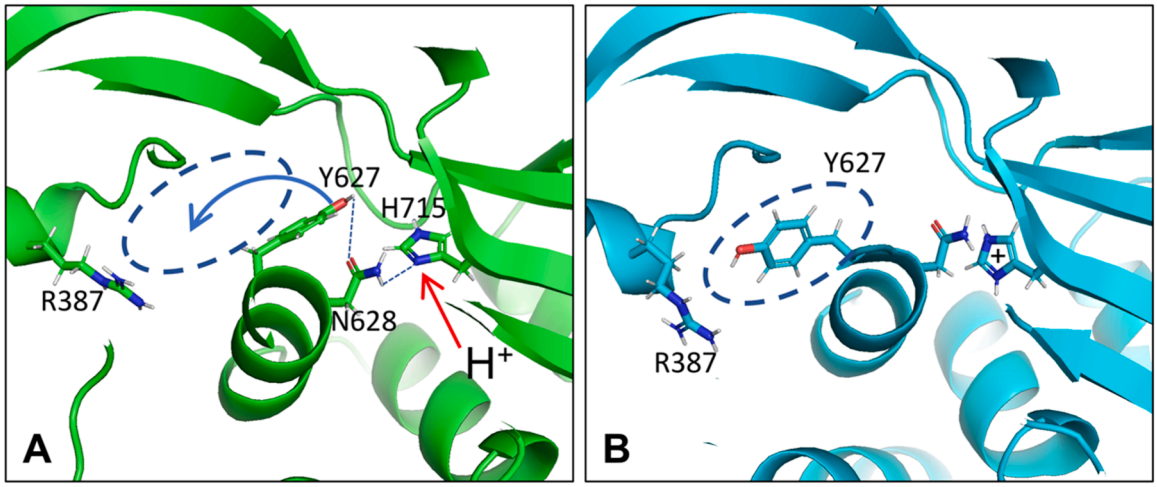

Fig. 4. Proposed mechanism for acid activation of *D. melanogaster* IR64a. A) Open state of LBD. Tyrosine 627 OH is H-bonded to Asparagine 628 which is H-bonded to Histidine 715. Ligand-binding site (dashed oval) is empty. B) Closed state of LBD. H^+ has bound to Histidine 715, breaking H-bond to Asparagine 628 and releasing Tyrosine 627, which rotated into ligand-binding site. This change is proposed to trigger ion channel opening.

Table 3
Ligand docking to *D. melanogaster* ionotropic receptors.

Receptor	LBD State	Predicted molecular docking sites[a]					
		Ligand site		Side site		Other	
		Ligand	ΔG°	Ligand	ΔG°	Ligand	ΔG°
*Dm*IR20a	Open	phenylalanine	-5.9	-		-	
		DEET	-6.1				
		IR3535	-4.9				
	Closed	phenylalanine	-6.3	-		-	
		DEET	-5.8				
		IR3535	-5.3				
*Dm*IR64a	Open	-		-		picaridin	-6.1
						citronellal	-5.3
						2-undecanone	-4.9
	Closed	-		picaridin	-5.9	-	
				citronellal	-5.3		
				2-undecanone	-4.8		

Footnotes: a) Ligand site and Side site: see Fig. 5. ΔG°: standard free energy change of ligand binding in Kcal/mol, based on AutoDock molecular docking analysis.

bind to the closed state. Representative binding free energy changes are shown in Table 4. The docking results suggest that *Isca*IR119 is a receptor that signals attraction. The mechanism by which the repellent menthanediol is excluded from the closed state is not known. It is possible that a repellent bound to the open state of the LBD stabilizes the open conformation and inhibits the transition to the closed state, thereby preventing attraction, which is a kind of repellency. The region of the closed state of *Isca*IR141 corresponding to the ligand binding site does not appear to bind any of the tested substances, either attractants or repellents, so it isn't possible to predict the valence of this receptor (Table 4). However, attractants and repellents were predicted to bind to surface regions of the open state near and to the right of where the closed-state binding pocket forms (Table 4 and Fig. 5). If DEET binding stabilizes the open state, this would inhibit signaling by *Isca*IR141.

4. Discussion

The computational analyses in this report advance our understanding of ligand binding to insect and tick chemosensory receptors. For a sample of eighteen *D. melanogaster* ORs and GRs, of which nine stimulate attraction and nine trigger aversion, all were predicted to bind DEET. Many of the DEET sites were located at the same internal site that ion channel triggering ligands bind, including more than half of the receptors for attractive ligands (Fig. 2, Table 1). This result is consistent with the idea that repellents like DEET act as "confusants" by sending contradictory signals to the insect brain (Pellegrino et al., 2011; DeGennaro, 2015). However, there is an alternative explanation involving the access tunnels that connect the occluded OR ligand binding sites to the receptor surface (Renthal and Chen, 2022). The tunnels are gated by transient bottlenecks that may act as size filters, and the tunnels have turns that may select for molecular flexibility. As shown in Table 2 and Fig. 3, the repellents that bind to attractant sites are larger and less flexible than the attractants. It is known that DEET, by itself, does not activate *Dmel*OR59b (Pellegrino et al., 2011), although the ligand binding site can accommodate DEET (Table 1). The structural model of *Dmel*OR59b (Fig. 1) shows a very narrow constriction between the ligand binding site and the exterior surface of the receptor. This constriction could act as a filter to exclude DEET and other repellents from the binding site. In future experiments, the role of the access tunnels could be tested by mutagenesis of tunnel-lining amino acids to smaller or larger side chains that could alter access. If many of the potential DEET sites, in ORs that activate attraction, are actually inaccessible to DEET, it would mean that DEET repellency may arise from a kind of OR summation: more OR ligand sites are accessible to DEET on repellent ORs than attractant ORs, so the behavioral response sums to aversion. The view that aversion versus attraction involves some kind of summation of OR signals is supported by the observation that when all Orco-containing neurons are optogenetically activated, the behavioral result is attraction (Guo et al., 2020; Tumkaya et al., 2022). If the "confusant" idea is correct for all combinations of attractive and aversive ORs, one would predict the optogenetic result of activating all Orco neurons should have been aversion.

In *D. melanogaster*, many ligands that activate particular IRs have been identified (Silbering et al., 2011; Munch and Galizia, 2016), but there is far less information about what behavioral responses are elicited. For *I. scapularis*, the IRs expressed in the Haller's organ are yet to be deorphanized, and there is little information about olfactory activity of particular ligands (Faraone et al., 2020; Josek et al., 2021). The modelling results reported here show evidence that in both *D. melanogaster* and *I. scapularis* there are IRs that may bind both attractants and repellents. As far as it is known, the ligand-binding sites in IRs are accessed through the open state of the LBD clam shell, which occurs in the receptors that have closed ion channels. This is unlike the ligand binding sites of many ORs which, by analogy with *Mhra*OR5, are occluded in receptors that have closed ion channels. Therefore, the possibility of a size and flexibility filter would seem to be applicable only

Table 4
Ligand docking to *I. scapularis* ionotropic receptors.

Receptor	LBD State	Predicted molecular docking sites[a]					
		Ligand site		Side site		Other site	
		Ligand	ΔG°	Ligand	ΔG°	Ligand	ΔG°
*Is*IR119	Open	p-cresol	-5.0	-		-	
		butyrate	-3.9				
		valerolactone	-4.5				
		citronellal	-4.8				
		2-undecanone	-5.4				
	Closed	p-cresol	-5.0	-		-	
		butyrate	-3.9				
		valerolactone	-4.6				
		citronellal	-5.6				
		2-undecanone	-5.1				
*Is*IR141	Open	p-cresol	-5.5	picaridin	-5.3	-	
		butyric acid	-4.2	citronellal	-4.6		
		valerolactone	-4.4	DEET	-5.8		
		menthanediol	-5.5	2-undecanone	-4.6		
	Closed	-		picaridin	-4.9	citronellal	-4.6
						DEET	-6.1
						2-undecanone	-4.4
						p-cresol	-5.4
						butyric acid	-4.5
						valerolactone	-4.3
						menthanediol	-5.8

Footnotes: a) Ligand site and Side site: see Fig. 5. ΔG°: standard free energy change of ligand binding in Kcal/mol, based on AutoDock molecular docking analysis.

to ORs and not IRs. For IRs that bind both attractants and repellents, decoding of competing signals into a behavioral response would have to be accomplished at the combinatorial level in the brain (Haverkamp et al., 2018). As a consequence, *a priori* prediction of repellent activity in acari may be more difficult than in insects, which have fewer IRs than ORs. A further complication in IRs is the presence of what may be an allosteric site to the side of the ligand-binding site. Repellents binding to the side site could control the ion channel by locking the open or closed LBD conformation. The deorphanization of tick IRs may be facilitated by the apparent independence of the LBD, which can be analyzed for binding activity while separated from the rest of the receptor (Kuusinen et al., 1995; Armstrong and Gouaux, 2000).

The model of *Dmel*IR64a suggests a mechanism for activation by H^+ binding to His 715 (Fig. 4). This histidine residue and the other key amino acids in the model (Tyr 627, Asn 628, and Arg 387) are conserved in Diptera, including the agricultural pests *Ceratitis capitata* (medfly) and *Calliphora stygia* (brown blowfly) and the disease vectors *Glossina fuscipes* (tsetse), *Anopheles gambiae* (African malaria mosquito) and *Aedes aegypti* (yellow fever mosquito) (Fig. 6), although in the latter two species Asn 628 is substituted with a serine residue, which presumably can perform a similar H-bonding function as proposed for asparagine. Repellents bind to a closed state site on the *Dmel*IR64a LBD surface adjacent to the ligand binding site (Side site, Table 3 and Fig. 5). If occupancy of this binding site stabilizes the closed state, it may be possible to use fluorescent dye-tagged LBDs in high-throughput binding screens to discover new species-specific repellents (Rajab et al., 2021).

The results reported here are based on computational analysis, using molecular models and ligand docking. Protein structure models derived from deep learning algorithms, such as AlphaFold2 (Jumper et al., 2021) or RoseTTAFold (Baek et al., 2021), are generally excellent, but there are serious questions about their suitability for docking studies. First, the proper model for insect ORs and arthropod IRs should be a heterotetramer containing tuning receptors and co-receptors. The AlphaFold models available from Uniprot are individual subunits, not oligomers. Oligomers can be custom-modeled, but it would add considerable complexity to the computational pipeline, even for a small receptor sample like Tables 1, 3 and 4. Second, the function of a ligand-gated ion channel necessarily involves conformational changes, but it is not clear which conformational states are produced by deep learning algorithms. The first concern, about oligomeric structures, is probably not significant for ligand docking studies of ORs and IRs. It has been experimentally demonstrated that individual subunits of the tuning receptors bind to known ligands in the absence of the co-receptor subunits (Kuusinen et al., 1995; Murugathas et al., 2019; Cheema et al., 2021). The second question, about the models' conformational state, does not appear to be a problem for ORs, nearly all of which were predicted by AutoDock to bind ligands at an interior site analogous to the eugenol binding site in *Mhra*OR5 (Table 1). However, the LBD of IRs exists in two very different

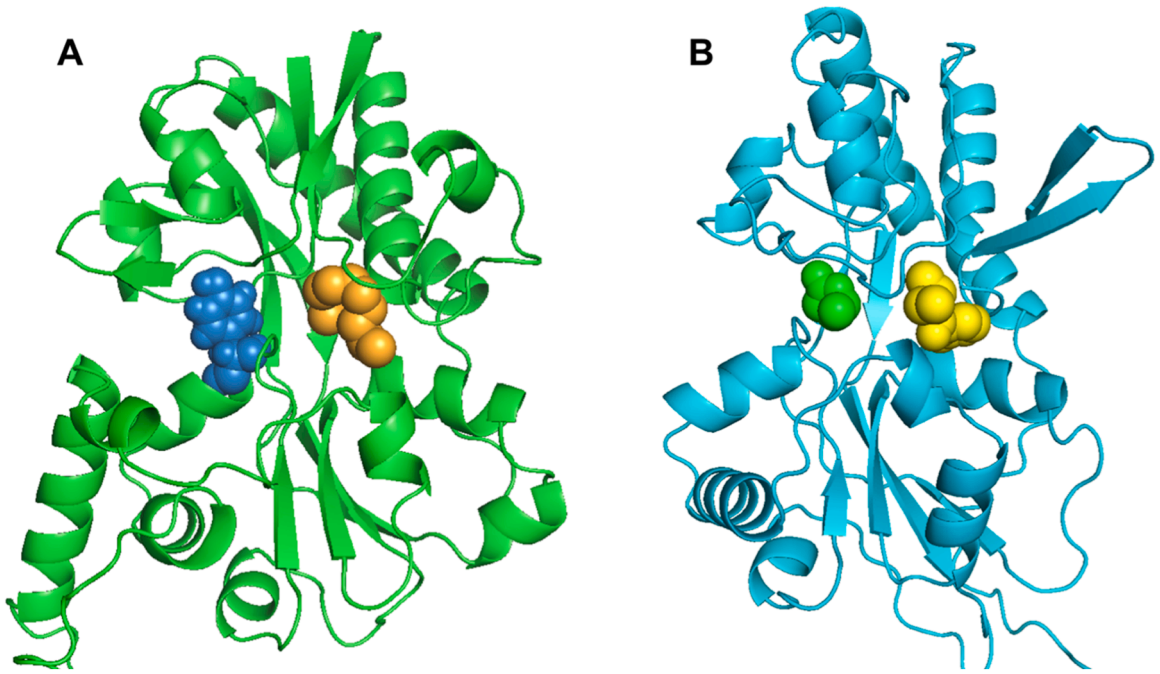

Fig. 5. Secondary structure cartoons of IR ligand-binding domains showing binding sites. A) *D. melanogaster* IR64a in closed conformation. Space-filling molecules: Tyr 627 (blue) in ligand-binding site; 2-undecanone (orange) in side site. B) *I. scapularis* IR141 in open conformation. Space-filling molecules: valerolactone (green) in ligand-binding site; DEET (yellow) in side site.

```
                                                                    ↓
D. melanogaster      334  LLMAVRDMFNWTFVLSRTTSWGYVKNGRFDGMIGALIRNETDIGGAPIFYWLERHKWIDV
C. capitata          674  LLSNVRDLYNFSFVMSKTASWGYLKNGKFDGMIGALVRKQADIGGSPIFFRIERAKVIDY
G. fuscipes          616  LLSNVRDLFNFSFILSKTSSWGYLKNGKFDGMIGALVRKQADIGGSPIFFRIERAKVIDY
C. stygia            770  LLTHVRDLFNFSFILSKTATWGYLKNGKFDGMIGALVRKQADIGGSPIFFRIERAKVIDY
A. aegypti           380  LMSYLKDYFNFRFIMRRTKSWGYLRNGTFDGMIGALARREVDLGGSPMFFRQERHRVVSY
A. gambiae            80  LMGMLKEFYNFTFVNRRTKSWGYLRNGKFDGMIGALSRREVDLGGSPMFFRQERHRVVSY

                                                  ↓
D. melanogaster      590  FYSASIVGTLLMEKPKTIKTLSDLVHSSLKVGMEDILYNRDYFLHTKDPVSMELYAKKIT
C. capitata          963  FYSASIVGTLLMEKPKTIRTLRDLIHSSLAVGVEDIPYNRDYFLRTKDPIAIELYAKKVT
G. fuscipes          856  FYSASIVGTLLMEKPKTIRTLRDLIHSSLEIGIEDIAYNRDYFLRTKDPVAQELYAKKVT
C. stygia           1000  FYSASIVGTLLMEKPKTIRTLRDLIHSNLEIGVEDIVYNRDYFLRTKDPDAQELYAKKVT
A. aegypti           738  YYSATIVGSLLMVPPKNIRTIRNLIDSKLTLGIEDIPYSRDYFV----------------
A. gambiae           328  YYSASIVGTLLMEQPKSIKTLRNLIDSRLTLGIEDIPYSRDYFVVSDCFISMDPAKIVLQ

                                  ↓
D. melanogaster      700  LDPETGLL--RHLGFAFHVDVAAAYKIIAETFSEQDICDLTEVSMFPP--QKTVSIMQKN
C. capitata         1082  YDPEYGVKRIRRGKFAFHVDVATAYKIIADTFNEKEICDLTEIQLFPP--QKMVNIVQKG
G. fuscipes          971  YDPDFGVNKIKKGRFAFHVDVATAYKIIADTYTEKEICDLTEIQLFPP--QKMVSIVQKG
C. stygia           1116  YDPDFGVAKIKKGRFAFHVDVATAYKIIADTFSEKEICDLTEIQLFPP--QKMVSIVQKG
A. aegypti           811  LNAADGLALVKAGGYAFHVAVSAGYKIIRETFSEREVCELAEIDMFPKSAQWMVAIVQKN
A. gambiae           435  LAAADGLQLVREGGYAFHVAISAAYRIIRLTFSEREICELSEIDMFPVWSQWMVAIVQKN
```

Fig. 6. Amino acid sequence comparisons of Dipteran IR64a homologs. Amino acids that are shown in the proposed acid-sensing mechanism (Fig. 4) are highlighted in red and indicated with an arrow. The starting sequence position of the first amino acid in each block is written to the left of the sequences. The sequence identifiers from the National Center for Biotechnology Information are, in order of listing: NP_647962.1, XP_023158641.1, XP_037881086.1, AID61277.1, NP_001345126.1, XP_315013.4.

conformational states. Surprisingly, all of the AF models of LBDs appeared to be in the open state, and many of the RF models of LBDs appeared to be in the closed state. This may reflect differences in the network architectures of the modeling algorithms, discussed by Baek et al. (2021). The favoring by AF of the open (or apo) conformation contrasts with a recent survey of 91 apo/holo pairs of AF models that found 67 % of the structures were similar to the holo (ligand-bound) structure (Saldaño et al., 2022). There is increasing interest in the issue of multiple protein conformational states in A.I. modeling (Sala et al., 2023; Wayment-Steele et al., 2023), and further work on this is likely to produce improved computational tools.

CRediT authorship contribution statement

Not applicable to a single-author paper.

Declaration of competing interest

The authors declare that they have no known competing financial interests or personal relationships that could have appeared to influence the work reported in this paper.

Data availability

Table 1. All molecular models listed in Table 1 for ligand docking calculations are publically available on UniProt (https://www.uniprot.org/), using the UniProt sequence IDs given in Supplementary Material 1 Table S1. The AutoDock Vina command lines used for calculation of the docking free energy changes shown in Table 1 are provided in Supplementary Material 4, along with the Vina output, which gives both the free energy change and the predicted atomic coordinates of the ligand docked to the protein. Tables 3 and 4. The molecular models of IR ligand-binding domains were obtained by running AlphaFold2 on local servers, or RoseTTAFold running on the Robetta web site (https://robetta.bakerlab.org/). The atomic coordinates are given in Supplementary Material 2. The determination of the conformational states of the ligand-binding domains was done as described in the Methods section. The ξ_1 and ξ_2 center of mass coordinates are given in Supplementary Material 3, along with the formula used for calculating the open/closed distances (shown in Table S1). The VMD Tk Console command lines for calculating the centers of mass, and the outputs, are given in Supplementary Material 4. The AutoDock Vina command lines used for calculation of the docking free energy changes shown in Tables 3 and 4 are provided in Supplementary Material 4, along with the Vina output, which gives both the free energy change and the predicted atomic coordinates of the ligand docked to the protein.

Supplementary materials

Supplementary material associated with this article can be found, in the online version, at doi:10.1016/j.cris.2024.100082.

References

Afify, A., Betz, J.F., Riabinina, O., Lahondere, C., Potter, C.J., 2019. Commonly used insect repellents hide human odors from anopheles mosquitoes. Curr. Biol. 29 (21), 3669–3680. https://doi.org/10.1016/j.cub.2019.09.007 e3665.

Ai, M., Min, S., Grosjean, Y., Leblanc, C., Bell, R., Benton, R., et al., 2010. Acid sensing by the Drosophila olfactory system. Nature 468 (7324), 691–695. https://doi.org/10.1038/nature09537.

Ai, M., Blais, S., Park, J.-Y., Min, S., Neubert, T.A., Suh, G.S.B, 2013. Ionotropic glutamate receptors IR64a and IR8a form a functional odorant receptor complex in vivo in Drosophila. J. Neurosci. 33 (26), 10741–10749. https://doi.org/10.1523/JNEUROSCI.5419-12.2013.

Armstrong, N., Gouaux, E., 2000. Mechanisms for activation and antagonism of an AMPA-sensitive glutamate receptor: crystal structures of the GluR2 ligand binding core. Neuron 28 (1), 165–181. https://doi.org/10.1016/s0896-6273(00)00094-5.

Badel, L., Ohta, K., Tsuchimoto, Y., Kazama, H., 2016. Decoding of context-dependent olfactory behavior in drosophila. Neuron 91 (1), 155–167. https://doi.org/10.1016/j.neuron.2016.05.022.

Baek, M., DiMaio, F., Anishchenko, I., Dauparas, J., Ovchinnikov, S., Lee, G.R., et al., 2021. Accurate prediction of protein structures and interactions using a three-track neural network. Science (1979) 373 (6557), 871–876. https://doi.org/10.1126/science.abj8754.

Brown, E.B., Patterson, C., Pancoast, R., Rollmann, S.M., 2017. Artificial selection for odor-guided behavior in Drosophila reveals changes in food consumption. BMC. Genomics. 18 (1), 867. https://doi.org/10.1186/s12864-017-4233-1.

Butterwick, J.A., Del Marmol, J., Kim, K.H., Kahlson, M.A., Rogow, J.A., Walz, T., et al., 2018. Cryo-EM structure of the insect olfactory receptor Orco. Nature 560 (7719), 447–452. https://doi.org/10.1038/s41586-018-0420-8.

Cheema, J.A., Carraher, C., Plank, N.O.V., Travas-Sejdic, J., Kralicek, A., 2021. Insect odorant receptor-based biosensors: current status and prospects. Biotechnol. Adv. 53, 107840 https://doi.org/10.1016/j.biotechadv.2021.107840.

Chen, Y.-C.D., Dahanukar, A., 2017. Molecular and cellular organization of taste neurons in adult Drosophila pharynx. Cell Rep. 21, 2978–2991. https://doi.org/10.1016/j.celrep.2017.11.041.

Dautel, H., Dippel, C., Werkhausen, A., Diller, R., 2013. Efficacy testing of several Ixodes ricinus tick repellents: different results with different assays. Ticks. Tick. Borne Dis. 4 (3), 256–263. https://doi.org/10.1016/j.ttbdis.2012.11.007.

DeGennaro, M., 2015. The mysterious multi-modal repellency of DEET. Fly. (Austin) 9 (1), 45–51. https://doi.org/10.1080/19336934.2015.1079360.

Del Marmol, J., Yedlin, M.A., Ruta, V., 2021. The structural basis of odorant recognition in insect olfactory receptors. Nature 597 (7874), 126–131. https://doi.org/10.1038/s41586-021-03794-8.

Doyle, D.A., Morais Cabral, J., Pfuetzner, R.A., Kuo, A., Gulbis, J.M., Cohen, S.L., et al., 1998. The structure of the potassium channel: molecular basis of K+ conduction and selectivity. Science (1979) 280 (5360), 69–77. https://doi.org/10.1126/science.280.5360.69.

Faraone, N., Light, M., Scott, C., MacPherson, S., Hillier, N.K., 2020. Chemosensory and behavioural responses of ixodes scapularis to natural products: role of chemosensory organs in volatile detection. Insects. 11 (8) https://doi.org/10.3390/insects11080502.

Ganguly, A., Pang, L., Duong, V.-K., Lee, A., Schoniger, H., Varady, E., Dahanukar, A., 2017. A molecular and cellular context-dependent role for Ir76b in detection of amino acid taste. Cell Rep. 18, 737–750. https://doi.org/10.1016/j.celrep.2016.12.071.

Guo, H., Kunwar, K., Smith, D, 2020. Multiple channels of DEET repellency in Drosophila. Pest. Manage Sci. 76 (3), 880–887. https://doi.org/10.1002/ps.5592.

Haverkamp, A., Hansson, B.S., Knaden, M., 2018. Combinatorial codes and labeled lines: how insects use olfactory cues to find and judge food, mates, and oviposition sites in complex environments. Front. Physiol. 9, 49. https://doi.org/10.3389/fphys.2018.00049.

Humphrey, W., Dalke, A., Schulten, K., 1996. VMD - Visual molecular dynamics. J. Mol. Graphics 14 (1), 33–38.

Josek, T., Sperrazza, J., Alleyne, M., Syed, Z., 2021. Neurophysiological and behavioral responses of blacklegged ticks to host odors. J. Insect Physiol. 128, 104175 https://doi.org/10.1016/j.jinsphys.2020.104175.

Josek, T., Walden, K.K.O., Allan, B.F., Alleyne, M., Robertson, H.M., 2018. A foreleg transcriptome for Ixodes scapularis ticks: candidates for chemoreceptors and binding proteins that might be expressed in the sensory Haller's organ. Ticks. Tick. Borne Dis. 9 (5), 1317–1327. https://doi.org/10.1016/j.ttbdis.2018.05.013.

Joseph, R.M., Carlson, J.R., 2015. Drosophila Chemoreceptors: a Molecular Interface Between the Chemical World and the Brain. Trends. Genet. 31 (12), 683–695. https://doi.org/10.1016/j.tig.2015.09.005.

Joseph, R.M., Sun, J.S., Tam, E., Carlson, J.R., 2017. A receptor and neuron that activate a circuit limiting sucrose consumption. Elife 6, e24992. https://doi.org/10.7554/eLife.24992.

Jumper, J., Evans, R., Pritzel, A., Green, T., Figurnov, M., Ronneberger, O., et al., 2021. Highly accurate protein structure prediction with AlphaFold. Nature 596 (7873), 583–589. https://doi.org/10.1038/s41586-021-03819-2.

Koh, T.-W., He, Z., Gorur-Shandilya, S., Menuz, K., Larter, N.K., Stewart, S., Carlson, J.R., 2014. The Drosophila IR20a clade of ionotropic receptors are candidate taste and pheromone receptors. Neuron 83, 850–865. https://doi.org/10.1016/j.neuron.2014.07.012.

Kuusinen, A., Arvola, M., Keinanen, K., 1995. Molecular dissection of the agonist binding site of an AMPA receptor. EMBO J. 14 (24), 6327–6332. https://doi.org/10.1002/j.1460-2075.1995.tb00323.x.

Lau, A., Roux, B., 2007. The Free energy landscapes governing conformational changes in a glutamate receptor ligand-binding domain. Structure 15, 1203–1214. https://doi.org/10.1016/j.str.2007.07.015.

Lee, Y., Kim, S.H., Montell, C., 2010. Avoiding DEET through insect gustatory receptors. Neuron 67 (4), 555–561. https://doi.org/10.1016/j.neuron.2010.07.006.

Lei, J., Liu, Q., Kadowaki, T., 2019. Honey bee parasitic mite contains the sensilla-rich sensory organ on the foreleg tarsus expressing ionotropic receptors with conserved functions. Front. Physiol. 10, 556. https://doi.org/10.3389/fphys.2019.00556.

Leonovich, S.A., 2004. Phenol and lactone receptors in the distal sensilla of the Haller's organ in Ixodes ricinus ticks and their possible role in host perception. Exp. Appl. Acarol. 32 (1–2), 89–102. https://doi.org/10.1023/b:appa.0000018200.24760.78.

Mohamed, A.A.M., Retzke, T., Das Chakraborty, S., Fabian, B., Hansson, B.S., Knaden, M., et al., 2019. Odor mixtures of opposing valence unveil inter-glomerular crosstalk in the Drosophila antennal lobe. Nat. Commun. 10 (1), 1201. https://doi.org/10.1038/s41467-019-09069-1.

Morris, G.M., Huey, R., Lindstrom, W., Sanner, M.F., Belew, R.K., Goodsell, D.S., Olson, A.J., 2009. AutoDock4 and AutoDockTools4: automated docking with selective receptor flexibility. J. Comp. Chem. 30, 2785–2791.

Munch, D., Galizia, C.G., 2016. DoOR 2.0–comprehensive mapping of drosophila melanogaster odorant responses. Sci. Rep. 6, 21841. https://doi.org/10.1038/srep21841.

Murugathas, T., Zheng, H.Y., Colbert, D., Kralicek, A.V., Carraher, C., Plank, N.O.V., 2019. Biosensing with insect odorant receptor nanodiscs and carbon nanotube field-effect transistors. ACS. Appl. Mater. Interfaces. 11 (9), 9530–9538. https://doi.org/10.1021/acsami.8b19433.

Pellegrino, M., Steinbach, N., Stensmyr, M.C., Hansson, B.S., Vosshall, L.B., 2011. A natural polymorphism alters odour and DEET sensitivity in an insect odorant receptor. Nature 478 (7370), 511–514. https://doi.org/10.1038/nature10438.

Rajab, S., Bismin, L., Schwarze, S., Pinggera, A., Greger, I.H., Neuweiler, H., 2021. Allosteric coupling of sub-millisecond clamshell motions in ionotropic glutamate receptor ligand-binding domains. Commun. Biol. 4, 1056. https://doi.org/10.1038/s42003-021-02605-0.

Renthal, R., 2021. Arthropod repellents and chemosensory reception. In: Coats, J., Corona, C., Debboun, M. (Eds.), Advances in Arthropod Repellents. Elsevier Academic Press, Cambridge, MA, pp. 141–161.

Renthal, R., Chen, L.Y., 2022. Tunnel connects lipid bilayer to occluded odorant-binding site of insect olfactory receptor. Biophys. Chem. 289, 106862 https://doi.org/10.1016/j.bpc.2022.106862.

Robertson, H.M., 2015. The Insect Chemoreceptor Superfamily Is Ancient in Animals. Chem. Senses. 40 (9), 609–614. https://doi.org/10.1093/chemse/bjv046.

Rytz, R., Croset, V., Benton, R., 2013. Ionotropic receptors (IRs): chemosensory ionotropic glutamate receptors in Drosophila and beyond. Insect Biochem. Mol. Biol. 43 (9), 888–897. https://doi.org/10.1016/j.ibmb.2013.02.007.

Sala, D., Engelberger, F., Mchaourab, H.S., Meiler, J., 2023. Modeling conformational states of proteins with AlphaFold. Curr. Opin. Struct. Biol. 81, 102645 https://doi.org/10.1016/j.sbi.2023.102645.

Saldaño, T., Escobedo, N., Marchetti, J., Javier Zea, D., MacDonagh, J., Velez Rueda, A. J., Gonik, E., García Melani, A., Nechcoff, J.N., Salas, M.N., Peters, T., Demitroff, N., Fernandez Alberti, S., Palopoli, Fornasari, M.S., Parisi, G., 2022. Impact of protein conformational diversity on AlphaFold predictions. Bioinformatics. 38 (10), 2742–2748. doi:10.1093/bioinformatics/btac202.

Sánchez-Alcañiz, J.A., Silbering, A.F., Croset, V., Zappia, G., Sivasubramaniam, A.K., Abuin, L., Sahai, S.Y., Münch, D., Steck, K., Auer, T.O., Cruchet, S., Neagu-Maier, G. L., Sprecher, S.G., Yapici, N., Benton, R., 2018. An expression atlas of variant ionotropic glutamate receptors identifies a molecular basis of carbonation sensing. Nat. Commun. 9, 4252. https://doi.org/10.1038/s41467-018-06453-1.

Schneider, C.A., Rasband, W.S., Eliceiri, K.W., 2012. NIH Image to ImageJ: 25 years of image analysis. Nat. Methods 9 (7), 671–675. https://doi.org/10.1038/nmeth.2089.

Silbering, A.F., Rytz, R., Grosjean, Y., Abuin, L., Ramdya, P., Jefferis, G.S., et al., 2011. Complementary function and integrated wiring of the evolutionarily distinct Drosophila olfactory subsystems. J. Neurosci. 31 (38), 13357–13375. https://doi.org/10.1523/JNEUROSCI.2360-11.2011.

Sonenshine, D.E., Adams, T., Allan, S.A., McLaughlin, J., Webster, F.X., 2003. Chemical composition of some components of the arrestment pheromone of the black-legged tick, Ixodes scapularis (Acari: ixodidae) and their use in tick control. J. Med. Entomol. 40 (6), 849–859.

Studer, G., Rempfer, C., Waterhouse, A.M., Gumienny, R., Haas, J., Schwede, T., 2020. QMEANDisCo-distance constraints applied on model quality estimation. Bioinformatics. 36 (6), 1765–1771. https://doi.org/10.1093/bioinformatics/btz828.

Su, C.Y., Menuz, K., Carlson, J.R., 2009. Olfactory perception: receptors, cells, and circuits. Cell 139 (1), 45–59. https://doi.org/10.1016/j.cell.2009.09.015.

Syed, Z., Pelletier, J., Flounders, E., Chitolina, R.F., Leal, W.S., 2011. Generic insect repellent detector from the fruit fly Drosophila melanogaster. PLoS. One 6 (3), e17705. https://doi.org/10.1371/journal.pone.0017705.

Thoma, M., Hansson, B.S., Knaden, M., 2014. Compound valence is conserved in binary odor mixtures in Drosophila melanogaster. J. Exp. Biol. 217 (Pt 20), 3645–3655. https://doi.org/10.1242/jeb.106591.

Trott, O., Olson, A.J., 2010. AutoDock Vina: improving the speed and accuracy of docking with a new scoring function, efficient optimization, and multithreading. J. Comput. Chem. 31 (2), 455–461. https://doi.org/10.1002/jcc.21334.

Tumkaya, T., Burhanudin, S., Khalilnezhad, A., Stewart, J., Choi, H., Claridge-Chang, A, 2022. Most primary olfactory neurons have individually neutral effects on behavior. Elife 11. ARTN e71238.

Wayment-Steele, H.K., Ojoawo, A., Otten, R., et al., 2023. Predicting multiple conformations via sequence clustering and AlphaFold2. Nature. https://doi.org/10.1038/s41586-023-06832-9 in press.

Weiss, L.A., Dahanukar, A., Kwon, J.Y., Banerjee, D., Carlson, J.R., 2011. The molecular and cellular basis of bitter taste in Drosophila. Neuron 69 (2), 258–272. https://doi.org/10.1016/j.neuron.2011.01.001.

Wood, W.R., Leahy, M.G., Galun, R., Prestwich, G.D., Meinwald, J., Purnell, R.E., Payne, R.C., 1975. Phenols as pheromones of Ixodid ticks: a general phenomenon? J. Chem. Ecol. 1, 501–509.

Yakel, J.L., 2010. Gating of nicotinic ACh receptors: latest insights into ligand binding and function. J. Physiol. 588 (Pt 4), 597–602. https://doi.org/10.1113/jphysiol.2009.182691.